Energy transfer in the spatial evolution of double-wave-group focusing ⊘

Binzhen Zhou (周斌珍) ⓘ ; Kanglixi Ding (丁康礼玺) ⓘ ; Yi Xiao (肖义) ⓘ ; Lei Wang (王磊) ✉ ⓘ ;
Tianning Tang (唐天宁) ⓘ

Check for updates

View Online   Export Citation

Articles You May Be Interested In

Influence of uniform currents on nonlinear characteristics of double-wave-group focusing

Physics of Fluids (March 2024)

Spatial evolution of the double-wave-group focusing influenced by the co- and counter-propagating current

Physics of Fluids (May 2024)

Experimental study on the interactions between wave groups in double-wave-group focusing

Physics of Fluids (March 2023)

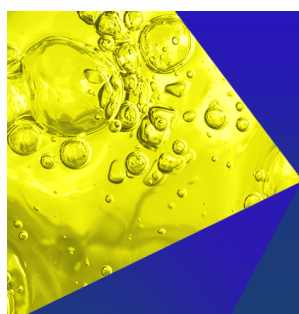Physics of Fluids

Energy transfer in the spatial evolution of double-wave-group focusing

View Online   Export Citation   CrossMark

Binzhen Zhou (周斌珍),[1,2] iD Kanglixi Ding (丁康礼玺),[2] iD Yi Xiao (肖义),[2] iD Lei Wang (王磊),[2,3,a] iD
and Tianning Tang (唐天宁)[4] iD

AFFILIATIONS

[1]State Key Laboratory of Subtropical Building and Urban Science, South China University of Technology, Guangzhou 510641, China
[2]School of Civil Engineering and Transportation, South China University of Technology, Guangzhou 510641, China
[3]Department of Civil and Environment Engineering, The Hong Kong Polytechnic University, Hong Kong 999077, China
[4]Department of Engineering Science, University of Oxford, Oxford, OX1 3PJ, United Kingdom

[a]Author to whom correspondence should be addressed: wangleimme@scut.edu.cn

ABSTRACT

The linear superposition of the individual wave groups underestimates the bimodal waves, as it overlooks the interactions between these wave groups, which is thought to be connected to the generation of extreme waves. Continuing our previous work [Zhou *et al.*, "Experimental study on the interactions between wave groups in double-wave-group focusing," Phys. Fluids **35**(3), 037118 (2023)], the energy transfer in the spatial evolution of double-wave-group focusing is highlighted based on a fully nonlinear numerical wave tank with the high-order spectral method. The findings reveal that a sea state with a narrower intermodal distance or an uneven distribution of the bimodal spectrum tends to induce larger waves. The third-order nonlinear interaction is primarily triggered by the transient wave focusing, as opposed to a prolonged evolution like the behavior of even-order components. The configurations of the sea state exert varying impacts on the evolution of harmonical energy, with the most potent nonlinearity observed away from the actual focused position, the nonlinear energy amplified relative to the initial state, and the energy redistributed after wave focus. The study also uncovers that during the wave focus and defocus process, waves experience an irreversible energy exchange, with frequencies shifting from higher to lower, likely due to second-order harmonics. These discoveries broaden our comprehension of the nonlinear characteristics inherent in the interaction between the swell and wind-sea waves.

I. INTRODUCTION

Bimodal sea states, which are common in actual marine environments with an occurrence probability as high as 30%,[2] have been proven to be more likely to generate extreme waves. Extreme waves, also known as freak waves, whose wave height is more than twice the significant wave height,[3] have been reported as a major responsibility for serious risk to the safety of marine activities.[4,5] Although the nonlinear characteristics at the focused position have been clearly explained, the total energy and the corresponding harmonical energy transfer in the spatial evolution are still unknown. To identify the impact of wave configurations on the occurrence of extreme waves, explore the spatial and temporal evolution patterns of double-wave-groups focusing, and explain the characteristics of harmonical energy transfer, is of significance to understand these nonlinear physics and enrich the theory of nonlinear wave dynamics.

In the bimodal sea state, the corresponding wave exhibits double peaks in the frequency spectrum. This typically happens when a wind-sea wave (with a relatively higher peak frequency) develops over a swell wave (with a relatively low peak frequency), resulting in double wave groups. Previous research has indicated that in the propagation of double-wave-group focusing, the nonlinear interaction primarily stems from two aspects,[1,6] interactions within a single wave group and interactions between different wave groups. Both of these are considered to be key drives in the generation of extreme waves.

Regarding the interactions within a single wave group, the physical mechanism behind extreme waves has been studied for several decades. It can be categorized into spatial and geometrical focusing,[7] abrupt depth transition,[8,9] wave-current interaction,[10,11] modulation instability,[12] and two or more of these effects worked simultaneously.[13–16] The spatial–temporal focusing is considered a key physical mechanism in the formation of extreme events. Rapp and Melville[17] proposed a phase-focusing method that could be used to reproduce the extreme waves in the experimental laboratory. Considering the nonlinear interaction, the actual focused amplitudes were found to exceed the assumed,[18] and the

actual focused positions were pointed out to deviate from that predicted by linear theory in both the numerical simulation and experiment.[19] Buldakov et al.[20] raised an iterative method to correct the deviation based on linear wave components obtained from the four-phase decomposition,[21] which is available to simulate the wave group focusing.[11] Additionally, the expansion of the wave amplitude was explained through some time-frequency conversion methods, such as the Fast Fourier Transform and Wavelet Transform.[22] The non-resonant[23] or resonance interaction[24] was proven to be associated with the energy transfer from the low frequency to the high frequency, contributing to the emergence of large waves.[25] The dispersion relation consequently varied, with some deviation from the theoretical prediction theory.[26]

In addition to the interactions within a single wave group, which are very common in the propagation of a single wave group, interactions between wave groups cannot be ignored. Tao et al.[27] found that the nonlinear interactions between wave groups can promote the magnitude of the water surface elevation in a long-term evolution of the modulational waves. In other theoretical research[6,28] and field analysis,[29,30] the same conclusion can be drawn. Rodriguez et al.[31] put forward two basic parameters to describe the spectral characteristics of a bimodal sea state, the intermodal distance (ID) and the sea-swell energy ratio (SSER). They pointed out that the wave configurations in the swell-dominated state (SSER < 1.00), the wind-sea-dominated state (SSER > 1.00), and the sea-swell energy equivalent state (SSER = 1.00) undergo different nonlinear physics, where the contribution of the second-order interaction was meaningful,[32] in particular, for a closer intermodal distance.[33] Moreover, Wang et al.[34,35] analyzed the influence of the configuration of the bimodal waves on the statistical properties utilizing the High-order Spectral method, demonstrating that ID and SSER have a significant impact on the nonlinear behaviors of the wave group, particularly for the condition with a closer intermodal (i.e., ID < 0.10) and an asymmetrical energy distribution (SSER ≠ 1.00), extreme waves is more prone to be generated. Additionally, an empirical model to predict extreme waves in the given bimodal sea state was fitted based on a large number of numerical simulations,[34] while the ignoring of the spatial and temporal evolution limits the applicability of the quantitative formula, even the waves with a larger steepness. In addition, the evolution of the double-wave-group focusing is preliminarily explored by utilizing the wavelet spectral method,[36] and the process by which the swell wave catches up to the wind-sea wave is shown. Furthermore, Zhou et al.[1] found that more second-order and third-order harmonics are activated at the focused position utilizing the harmonics analysis.

The impact of the sea state on the nonlinear interactions at the focused position has been explained. However, the evolution of these nonlinear interactions and the transfer of harmonical energy remains unclear. Therefore, we aim to numerically investigate the energy evolution during the process of the double-wave-group focusing. Our work brings three novel contributions. First, focused amplitudes with spectral distribution are compared and the configurations easier to motivate the large waves are identified. Second, the evolution of the harmonical energy is given based on the harmonics analysis. Third, the irreversible energy exchange in the wave focus and defocus is clarified.

The rest of this paper is arranged as follows. In Sec. II, the numerical modal and configurations of the bimodal sea state are briefly introduced. Section III illustrates the evolution characteristics in the time and frequency domain with various spectral distributions. Section IV analyzes the energy transfer in double-wave-group focusing. Finally, the conclusions are summarized in Sec. V.

II. NUMERICAL MODEL
A. Numerical wave tank

Double-wave-group focusing (corresponding to the bimodal sea state) undergoes such complex physical processes, which a fully nonlinear numerical model with an advantage in accuracy and efficiency is needed. There are several types of fully nonlinear numerical wave models currently in existence, such as computational fluid dynamics (CFD) based on the Navier–Stokes equation, boundary element method (BEM), or high-order spectral (HOS) method based on the Laplace equation, and so on. However, the CFD method not only suffers from numerical dissipation, making it difficult to accurately capture the free surface elevation but also requires a large number of grids leading to great limitations in computational efficiency. The BEM needs to solve the matrices with great computational complexity and high computational cost. By contrast, the HOS method solves the velocity potential and its derivative terms by Fast Fourier Transform (FFT), with a great advantage in efficiency as well as accuracy. It is preferred when solving extreme waves with strong nonlinearity, and it is successfully applied to simulating single-wave-group focusing,[37] double-wave-group focusing,[34,36] and even wave co-propagating with opposing current.[38]

In this study, a numerical wave model based on the High-order Spectral (HOS) method named HOS-NWT solver[39] is employed to collect the time series data of the water surface elevation in the double-wave-group focusing to be analyzed. Assuming the fluid is incompressible, inviscid, and irrotational, the velocity potential inside the domain, $\Phi(x, z, t)$ is divided into free surface velocity potential Φ_f and additional velocity potential Φ_{add}, also satisfying the Laplace equation[40]

$$\nabla^2 \Phi = 0 \quad \text{in } D, \tag{1}$$

where $\nabla = (\partial/\partial x, \partial/\partial z)$, D represents the fluid domain.

Analogous to the advanced HOS model, the free surface kinematic and dynamic boundary conditions are revised as[41,42]

$$\frac{\partial \eta}{\partial t} = \left(1 + \left|\frac{\partial \eta}{\partial x}\right|^2\right)\frac{\partial \Phi_f}{\partial z} + \frac{\partial \Phi_{add}}{\partial z} - \left(\frac{\partial \Phi_f}{\partial x} + \frac{\partial \Phi_{add}}{\partial x}\right)\frac{\partial \eta}{\partial x},$$
$$z = \eta(x, t),$$

$$\frac{\partial \Phi_f}{\partial t} = -\eta + \frac{1}{2}\left(1 + \left|\frac{\partial \eta}{\partial x}\right|^2\right)\left(\frac{\partial \Phi_f}{\partial z}\right)^2 - \frac{1}{2}\left|\frac{\partial \Phi_f}{\partial x}\right|^2$$

$$-\frac{1}{2}|\nabla\Phi_{add}|^2 - \frac{\partial \Phi_f}{\partial x}\cdot\frac{\partial \Phi_{add}}{\partial x} - \frac{\partial \Phi_{add}}{\partial t}, \quad z = \eta(x, t). \tag{2}$$

in which η denotes the surface elevation of the water wave.

The corresponding bottom and wavemaker boundary conditions are rewritten as

$$\frac{\partial \Phi}{\partial z} = \frac{\partial \Phi_f}{\partial z} + \frac{\partial \Phi_{add}}{\partial z} = 0, \quad z = -h, \tag{3}$$

$$\frac{\partial S}{\partial t} = \frac{\partial \Phi_{add}}{\partial x}, \quad x = 0, \tag{4}$$

where h denotes the water depth, and S is the displacement of the wavemaker.

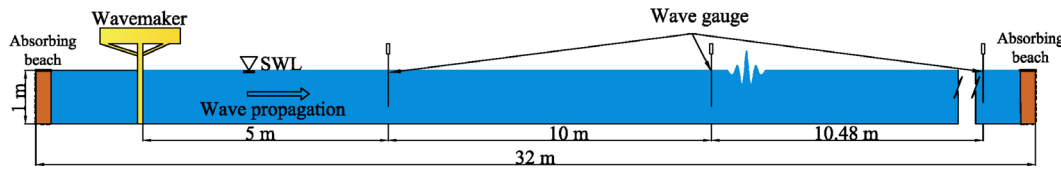<div style="writing-mode: vertical">27 November 2025 08:56:06</div>

FIG. 1. Sketch of the numerical wave tank.

Based on these boundary conditions, the calculation domain is initialized as

$$\begin{cases} \eta(x, t = 0) = 0, \\ \Phi_f(x, t = 0) = 0. \end{cases} \tag{5}$$

Φ_f satisfies the Laplace equation, the free surface boundary conditions, and the bottom boundary condition and can be expressed in a perturbation series up to the arbitrary nonlinear order solved by the Fast Fourier Transform according to the traditional HOS method.[41] Φ_{add} satisfies the Laplace equation, the wavemaker boundary condition, and the bottom boundary condition and can be obtained from the linear wavemaker theory.[43] After gaining all the terms on the right side of the rewritten boundary equations, the velocity potential and the free surface elevation in the next time step can be calculated through the time integration using the fourth-order Runge–Kutta method.

The numerical wave tank based on the HOS method is illustrated in Fig. 1. The wavemaker is located on the left side, and the absorbing zone is on the other side, with a working depth $h = 1.0$ m, and a horizontal length $L_x = 32$ m. The focused position and the focused time are assumed as $x_b = 15$ m and $t_b = 50$ s. A series of wave gauges are set away from the wavemaker from 5.0 to 25.48 m to record more time history information along the wave propagation.

B. Bimodal sea state

The iterative method proposed by Buldakov *et al.*[20] is comprised to correct the deviation of the actual focused position relative to the assumed focused position in single-wave-group focusing.

Subsequently, the linear superposition of two corrected wavemaker signals of the corresponding single wave group is adopted to generate the double-wave-group focusing. This method is also applied to the study of Zhou *et al.*[1] The validation of the method can be referred to Appendix A.

Generally, sea-swell energy ratio (SSER) and intermodal distance (ID) are the two major characteristics of the bimodal sea state,[31] characterizing the energy ratio of the swell system (low-frequency partition) and the wind-sea system (high-frequency partition) as well as the peak frequency space between them, respectively,

$$SSER = \frac{m_{02}^2}{m_{01}^2}, \tag{6}$$

$$ID = \frac{f_{p2} - f_{p1}}{f_{p1} + f_{p2}}, \tag{7}$$

where m_0 is the zero-order spectral moment, f_p represents the peak frequency, and subscripts 1 and 2 denote the swell and wind-sea systems, respectively.

13 cases with equivalent energy are chosen to be simulated, considering configurations with various values of SSER and ID, listed in Table I. The total number of wave components is fixed as 193, uniformly distributed in the same spectral range $\Delta f = 0.5 \sim 2.0$ Hz. A_b represents the assumed focused amplitude, and k_p represents the peak wavenumber corresponding to the peak frequency and can be obtained from the dispersion relation. Note that the steepness $k_p A_b$ of the equivalent single wave group is set as 0.15, which is defined as a moderate value not large enough to result in wave breaking. The corresponding input amplitude spectra are presented in Fig. 2.

TABLE I. Detailed configurations of the bimodal sea states.

| Case	A_{b1} (m)	f_{p1} (Hz)	$k_{p1}A_{b1}$	A_{b2} (m)	f_{p2} (Hz)	$k_{p2}A_{b2}$	ID	SSER
1	0.025	1.008	0.102	0.025	1.008	0.102	0.00	
2	0.025	0.956	0.092	0.025	1.057	0.112	0.05	
3	0.025	0.924	0.086	0.025	1.085	0.119	0.08	
4	0.025	0.903	0.082	0.025	1.103	0.122	0.10	1.00
5	0.025	0.791	0.063	0.025	1.186	0.142	0.20	
6	0.025	0.733	0.055	0.025	1.222	0.150	0.25	
7	0.032	0.984	0.123	0.016	1.331	0.113		0.25
8	0.027	0.899	0.089	0.022	1.216	0.133		0.67
9	0.026	0.876	0.082	0.024	1.185	0.133		0.80
10	0.025	0.847	0.073	0.025	1.146	0.132	0.15	1.00
11	0.024	0.821	0.065	0.026	1.111	0.131		1.25
12	0.022	0.803	0.059	0.027	1.087	0.130		1.50
13	0.016	0.755	0.037	0.032	1.022	0.133		4.00
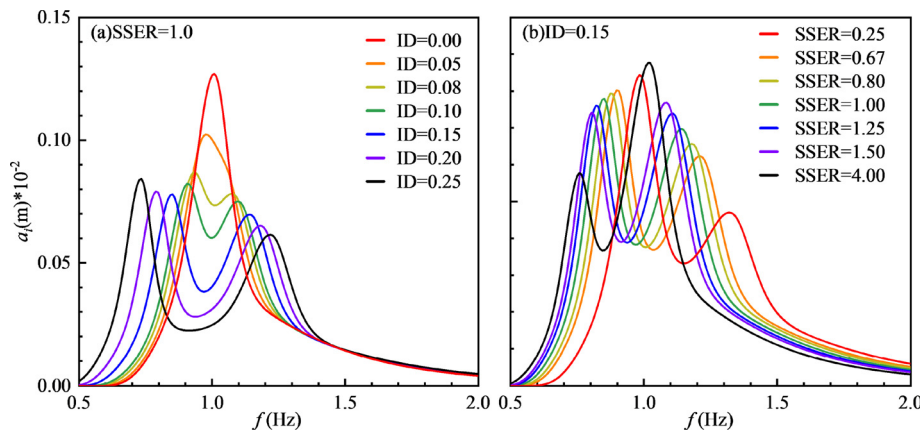
FIG. 2. Input amplitude spectra of the prescribed bimodal sea states, (a) with different values of ID and (b) with different values of SSER.

The established numerical wave tank is validated in Appendix B with the wave configuration of case 4 (ID = 0.1, SSER = 1.0), available for the coming simulations.

III. EVOLUTION CHARACTERISTICS IN TIME AND FREQUENCY WITH SPECTRAL DISTRIBUTIONS
A. Evolution of double-wave-group focusing

Due to the nonlinear interactions in the wave propagation, the actual focused position and the focused amplitude will deviate from the assumed. In our study, the actual focused position is defined as the

position that the largest crest reaches its maximum. For example, the actual focused position of case 5 in this section is at $x_{ab} = 15.2$ m. Figure 3 gives the evolutions of the double-wave-group focusing including wave surface elevation (represented by white lines) and the corresponding wavelet spectrum (represented by colored contours where the color bar represents the nondimensional wavelet energy ratio of energies relative to the maximal energy). Information is collected at five locations, namely, two before, one at, and two behind the actual focused position, respectively. λ_z is defined as the average zero-crossing wavelength obtained from T_z. A_b ($= A_{b1} + A_{b2}$) is the total
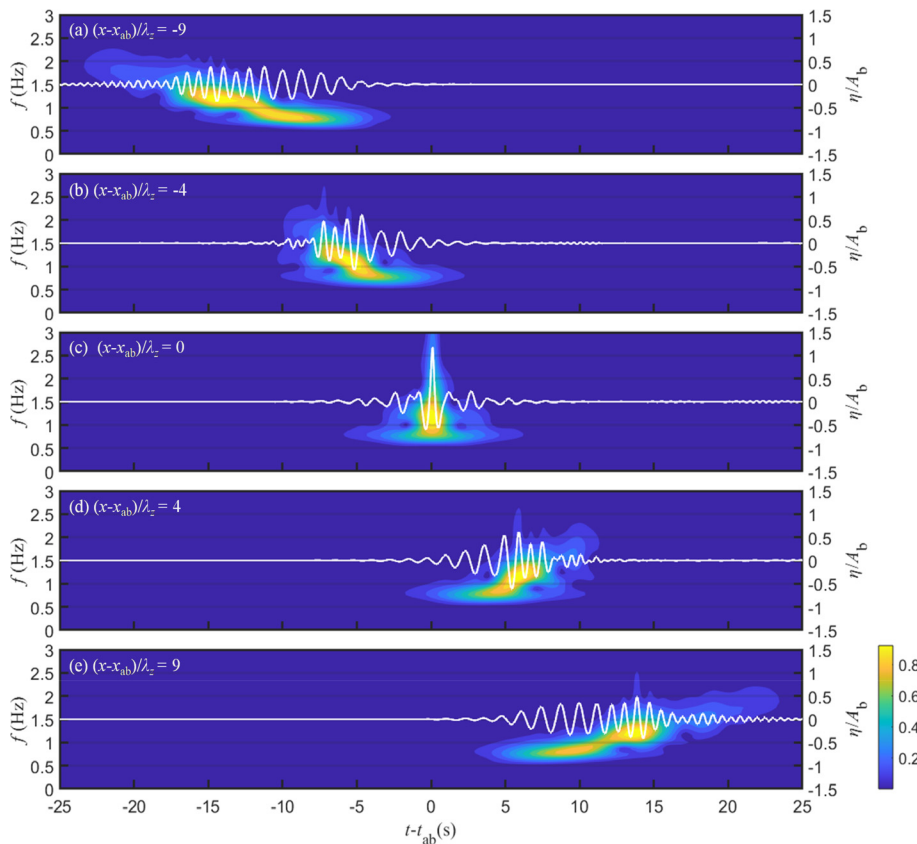

FIG. 3. Evolution of surface elevation and corresponding wavelet spectrum in the process of double-wave-group focusing (case 5: ID = 0.20, SSER = 1.00).

amplitude of double-wave-group focusing. Near the wavemaker [Fig. 3(a)], there are two separated wave groups with concentrated energy initially, long waves (with relatively high peak frequency) chasing short waves (with relatively low peak frequency). With the wave groups converging, high-order harmonics are gradually triggered. Till the actual focused position [Fig. 3(c)], the surface elevation reaches the maximum value, up to $\eta/A_b = 1.17$, and even the wavelet power emerges more high-frequency components presenting an inverted tri-angle shape. After the long waves surpass the short waves [Fig. 3(e)], the two wave groups gradually separate.

Although the overall process of focusing is like that of single wave group focusing, one very attractive phenomenon is that undergoing the wave group focusing, the two wave groups are different from the two before focusing. It indicates that the energies between the two wave groups are redistributed, which is worthwhile to conduct in-depth research in the following.

B. Wave surface elevation at focused position

The difference between Case AB and Case A + B has been pointed out to be associated with the interaction between wave groups, while that between Case A + B and linear theory is related to the inter-action within the single wave group.[1] Figure 4 analyzes the variation of the focused amplitude with various values of ID and SSER, including

η_{AB} relative to η_{A+B} [i.e., $(\eta_{AB})_{max}/(\eta_{A+B})_{max}$, represented by red squares] and η_{A+B} relative to linear theory [i.e., $(\eta_{A+B})_{max}/A_b$, represented by blue dots], to compare the impact of spectral distribution on these two interactions.

In Fig. 4(a), with the increase in ID, apparent discrepancies in the interactions between wave groups and those within the single wave group happen. $(\eta_{AB})_{max}/(\eta_{A+B})_{max}$ first falls rapidly and then trends stable, with values from 1.21 to 1.04, while $(\eta_{A+B})_{max}/A_b$ slightly increases. This is because, on one hand, as the peak frequency space increases, the wind-sea system becomes steeper (seen Table I) and its nonlinearity correspondingly enhances. This leads to a slight increase in $(\eta_{A+B})_{max}/A_b$, namely, a slight enhancement of the interactions within the single wave group, that is to say, the steeper the wave profile, the stronger the nonlinearity, the more sensitive the numerical model, and the more the significant nonlinear behavior. On the other hand, the larger the value of ID, the wider the spectral bandwidth, and the fewer wave components in the crossing region, inducing weaker inter-actions between the swell system and the wind-sea system.

Unlike the monochronic tendency with various values of ID, dif-ferent variations with SSER are illustrated in Fig. 4(b). Both $(\eta_{AB})_{max}/(\eta_{A+B})_{max}$ and $(\eta_{A+B})_{max}/A_b$ first decrease and then increase with the increase in SSER, except one point at SSER = 4.0. The minimum val-ues appear at SSER = 1.0, consistent with the variation of wave ampli-tude observed in the physical experiment[1] and maximum kurtosis
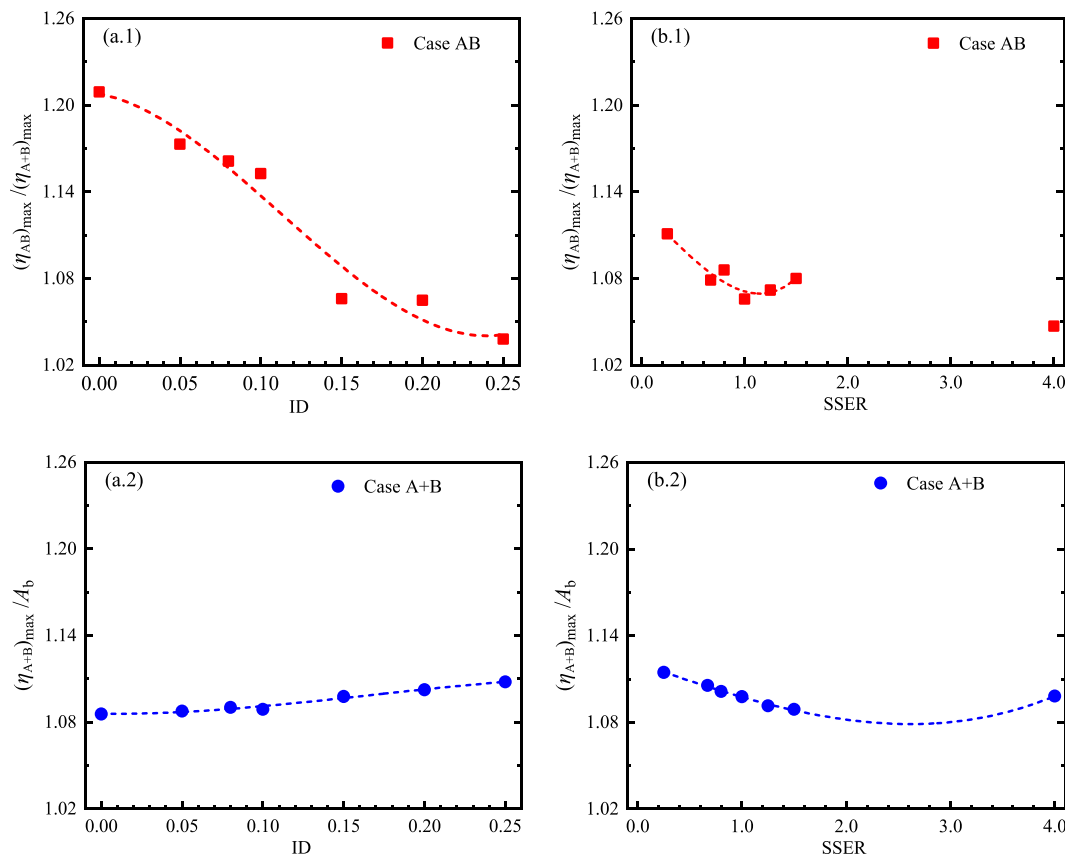

FIG. 4. Variations of focused amplitude in bimodal sea states with various values of ID (a) and SSER (b). (1) $(\eta_{AB})_{max}/(\eta_{A+B})_{max}$ and (2) $(\eta_{A+B})_{max}/A_b$.
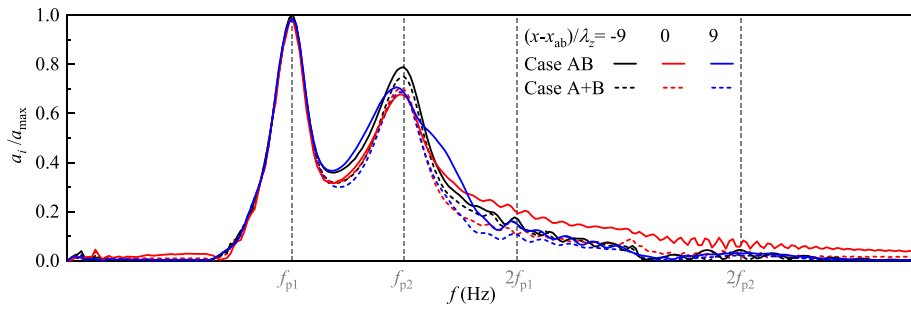
FIG. 5. Evolution of frequency spectra (case 5: ID $= 0.20$, SSER $= 1.00$).

statistics from the numerical results.[34] This proves that asymmetry spectral distributions promote the interaction between wave groups as well as the interaction within the wave group. The influence of ID and SSER on the nonlinear interaction manifests that the closer the inter-modal distance (smaller value of ID), the more disequilibrium the spectral distribution (SSER < 1.00 or SSER > 1.00), and the larger the focused amplitude, meaning the more components participated in the energy transfer.

C. Evolution of frequency spectra

Figure 5 compares the evolution of frequency spectra between Case AB (represents the sum of interactions within and between wave groups, marked with solid lines) and Case A + B (represents the interactions within wave groups, marked with dotted lines), taking one wave configuration as an example. In the figure, the vertical axis is normalized by the maximum value of the amplitude spectrum (namely, a_{max}) of Case A + B.

At the initial stage (at the position nine times the characteristic wavelength before the focused), the black solid line coincides with the black dotted line in the swell system (corresponding to the relatively low-frequency partition) but lies above the black dotted line in the wind-sea system (corresponding to the relatively high-frequency partition). It demonstrates that the interactions between wave groups begin to emerge at that moment. As the waves propagate to the focused position, their nonlinearity reaches the maximum, accompanied by a greater deviation between the red solid line and the red dotted line in the higher frequency region. These phenomena are consistent with our previous experimental study.[1] The enhancement of the interaction between wave groups activates more substantial nonlinearity, closed related to the increase in the focused amplitude of Case AB relative to Case A + B observed in Fig. 4(a.1). As the swell waves (relatively long waves) gradually surpass the wind-sea waves (relatively short waves), the energies in the fundamental frequency range tend to go back to the initial state, and those of the higher-order harmonics weaken. Yet, the energy in this state is not completely synchronized with the initial, although the propagation distance between these two stages is the same. Compared to Case A + B, it seems that more wave components are transferred to the wind-sea system for a local broadened bandwidth exhibited in Case AB, probably due to the presence of interactions between two wave groups. It suggests that nonlinear interactions in the process of double-wave-group focusing induce the redistribution of spectral energy in the process of focus and defocus with the same evolutionary distance.

IV. ENERGY TRANSFER IN DOUBLE-WAVE-GROUP FOCUSING

A. Evolution of total energy in time and space

To explain the evolution of energy in the process of double-wave-group focusing, the total energy of the numerically simulated waves should be given first, shown in Fig. 6 including temporal evolution
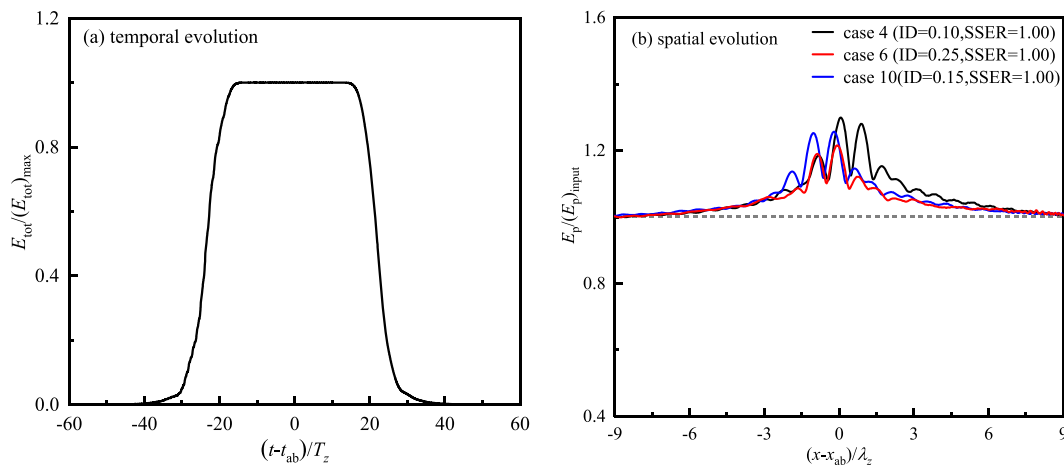

FIG. 6. Evolution of total energy in the process of double-wave-group focusing. (a) Temporal evolution and (b) spatial evolution.

[Fig. 6(a)] and spatial evolution [Fig. 6(b)], in which T_z is defined as the average zero-crossing period to describe the distribution of a bimodal sea state.[44]

From Fig. 6(a), it can be observed that after all components of the wave group are generated from the wavemaker and before being dissipated by the absorbing layer, the total energy remains constant for a long time, proving that the energy of the entire closed system is conserved. This means that with the propagation of a bimodal wave group, only kinetic energy and potential energy undergo mutual conversion. The corresponding variation of potential energy is given in Fig. 6(b). As approach the actual focused position, the potential energy gradually grows and exhibits bimodal behavior. Note that the maxima of the potential energy fails to be at the actual focused position, which does not conform to our conventional cognition. It is quite necessary to explore what exactly happens during the double-wave-group focusing consequently.

B. Evolution of harmonical energy

The harmonics analysis of the focused wave group can be conducted by utilizing the four-phase decomposition method.[21] Inspired by this, the total energy can be divided into four parts, representing the linear part (E_1), second-order sum part (E_2), third-order part (E_3), and second-order difference and fourth-order part (E_4), which has been successfully available in tracking the energy transfer in the focused process.[45,46] Figure 7 illustrates the spatial evolution of harmonic energy with various values of ID and SSER, in which the vertical axis represents the harmonic energy (E_i) normalized by the corresponding total potential energy (i.e., the energy sum of various order harmonics, that is, $E = E_1 + E_2 + E_3 + E_4$) and the horizontal axis $(x - x_{ab})/\lambda_z$ represents the number of the waves away from the actual focused position. The vertical dotted line represents the actual focused position, and the horizontal dotted line represents the initial harmonic energy of case 4 (ID = 0.10 and SSER = 1.00) in Fig. 7(a) and case 10 (ID = 0.15 and SSER = 1.00) in Fig. 7(b).

In Fig. 7, the overall spatial evolution of harmonical energy is quite similar irrespective of the energy ratio or the intermodal distance. In the initial stage of the wave propagation, the value of E_1/E weakly declines, accompanied by a little increase in E_2/E. When waves approach a position about three times the characteristic wavelength, higher-order nonlinear interactions can be motivated by sufficient evolution, with a sudden enhancement of E_2/E, E_3/E, and E_4/E and a sharp drop of E_1/E. Till near the focused position, the proportion of nonlinear energy is up to 30%. As the wave propagates away from the focused position, the proportion of the harmonic energy gradually approaches the initial state.

However, the state of the peak looks different, influenced by the energy ratio and intermodal distance. The behaviors of E_1/E exhibit bimodal, with a peak before and after the focused position. In Fig. 7(a.1), for configurations with smaller ID values (ID ≤ 0.10), as the value of ID becomes larger, the energy decreases in the fundamental frequency range, and the position where the peak energy appears lags further behind the focused position. For those with larger ID values (ID > 0.10), the maximum of fundamental energy occurs before the actual focused position, and the larger the value of ID, the larger the proportion of linear energy, and the smaller the deviation from the focused position. These mean that when the wind-sea partition and the swell partition have not yet been completely separated,[34,36] there

are interactions between wave groups resulting in a longer evolutionary distance and more high-frequency components. In Fig. 7(b.1), as the value of SSER becomes larger, the peak before the focused position as well as that behind the focused position gradually decreases and the decrease behind the focused position is more pronounced, reflecting that the more disequilibrium the energy distribution, the weaker the nonlinear interaction. The above phenomena can also be used to help explain the variation of nonlinear statistics observed in bimodal sea states with various energy ratios or with various intermodal distances.[30,35]

Additionally, although the proportion of the harmonic energy gradually approaches the initial state as the wave propagates away from the focused position, the energy does not completely return to the initialization. This indicates that the nonlinear interaction that occurs during the wave propagation is irreversible, which is the typical difference between lights and waves.

C. Properties of energy transfer

The complex interactions during wave propagation facilitate energy transfer, being an intrinsic trigger of wave profile. In the process of double-wave-group focusing, the maximum values of the harmonical energy do not occur at the actual focused position due to the high-order nonlinearity. To investigate the patterns of the variation, three parameters are used to describe the properties of energy transfer.

(1) Δ is defined as the deviation of the position with the strongest nonlinearity relative to the actual focused position, expressed as

$$\Delta = (x_e - x_{ab})/\lambda_z, \tag{8}$$

where x_e is the position corresponding to the peak point in the evolution of different harmonical energies.

(2) E_v is defined as the relative difference between the peak value and the initial value, to measure the maximum amplification in the process of harmonical energy evolution, written as

$$E_v = (E_e - E_L)/E_L, \tag{9}$$

where E_L and E_e represent the value of the harmonical energy at the prescribed initial position [i.e., $(x - x_{ab})/\lambda_z = -9$] and at the corresponding peak point, respectively.

(3) E_d is defined as the energy difference of the same evolutionary distance before and after the wave group focusing, to evaluate the symmetry of the energy transfer in the focusing process, given as

$$E_d = E_R - E_L, \tag{10}$$

where E_R represents the value of the harmonical energy at $(x - x_{ab})/\lambda_z = 9$.

1. Deviation of the position with the strongest nonlinearity

Figure 8 gives the deviation of the position with the strongest nonlinearity relative to the actual focused position in various configurations of double-wave-group focusing. In Fig. 8(a), when the values of ID are smaller than 0.10, the deviation of the position Δ presents positive, demonstrating that the peak value of each harmonical energy appears behind the actual focused position, and otherwise for larger
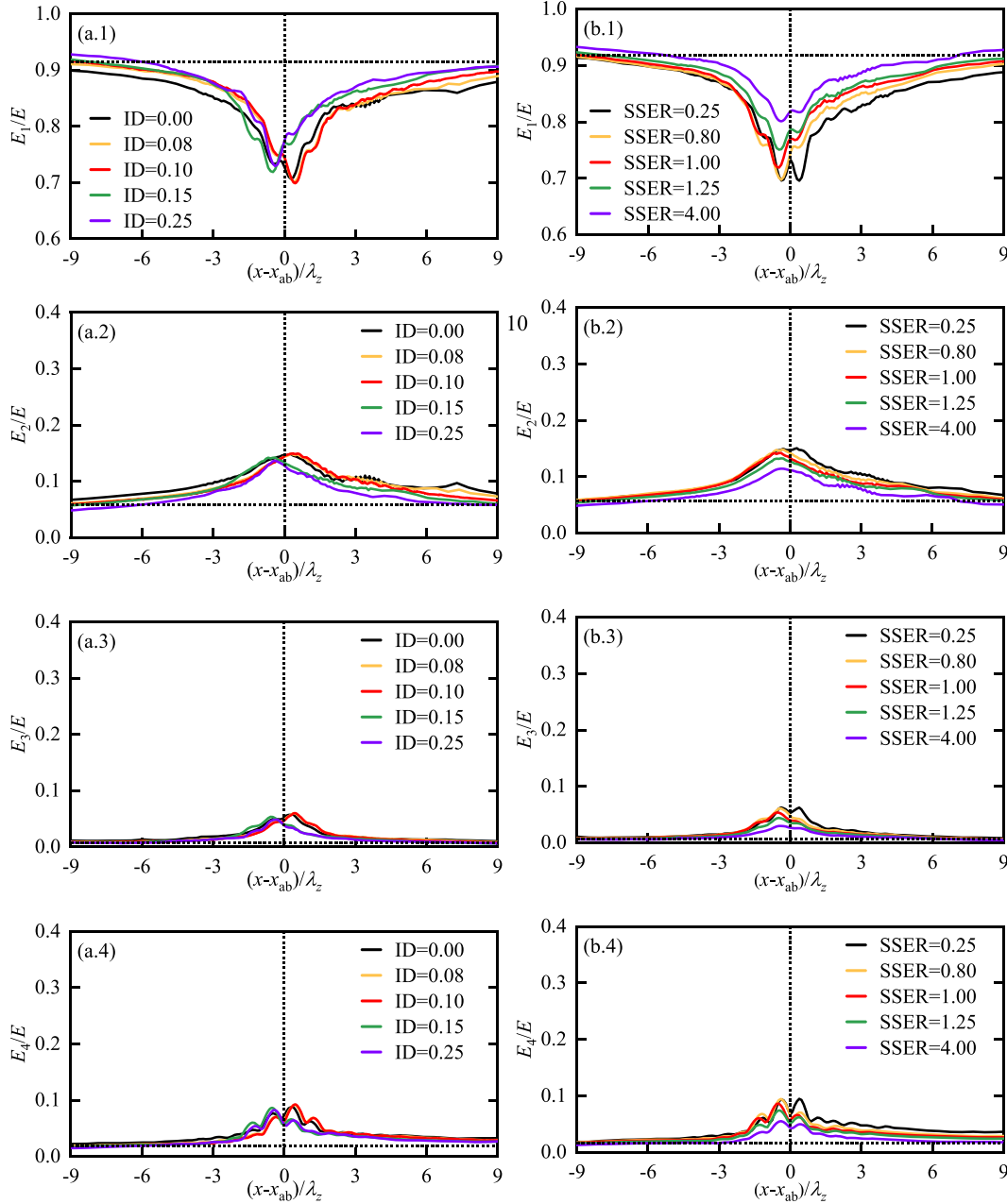
FIG. 7. Spatial evolution of harmonical energy in double-wave-group focusing with various values of ID (left: a) and SSER (right: b). (1) E_1/E, (2) E_2/E, (3) E_3/E, and (4) E_4/E.

values of ID. Meanwhile, the variation of E_1 and E_2 with ID is quite similar, both initially stabilizing or steadily increasing, and then gradually decreasing to stable when it reaches 0.10. While concerning E_3 and E_4, they are significantly reduced at the moment the ID becomes larger, showing greater sensitivity to the changes in the intermodal distance. In Fig. 8(b), when SSER equals 1.0, the deviations of the position with the strongest nonlinearity before the focused position reach the maximum except for that of the second-order sum (slightly earlier),

reflecting that the weakest nonlinearity happened in the wind-sea and the swell equivalent sea state is attributed to the combination of all wave components, although the effect of the second-order sum is minor. This is a little different from the observation by Wang et al.,[34] that the point SSER $= 1.0$ is the inflection point of nonlinear statistical parameters, with a minimum value. It is because the corresponding value of ID is different, the previous one with ID $= 0.10$ and here ID $= 0.15$, taking on different energy distribution. In a word, when the
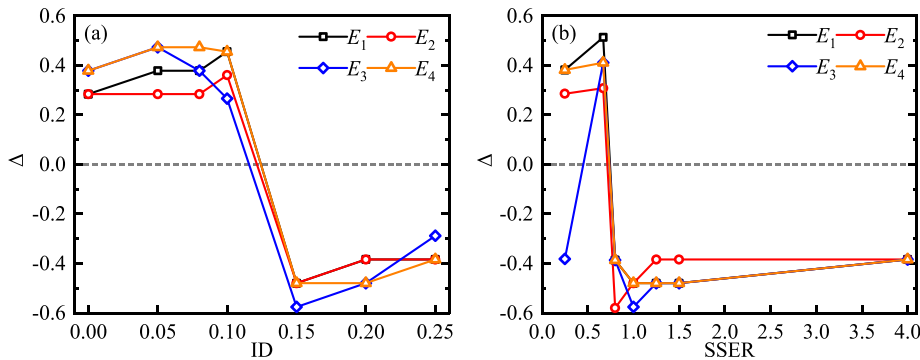
value of ID is lower than 0.10 or SSER lower than 0.67, the position where the strongest nonlinearity occurs is delayed relative to the actual focused one, but otherwise for the value of ID more than 0.10 or SSER more than 0.67.

2. Maximum amplification during the evolution of harmonical energy

The maximum amplification E_v in the process of harmonical energy evolution in various wave configurations is presented in Fig. 9.

In Fig. 9(a), with the increase in the intermodal distance, the energies of the nonlinearity (including E_2, E_3, and E_4) significantly grow up and the blue line (i.e., E_3) is always at the top along with the orange line (i.e., E_4) second. Till ID = 0.10, the amplification E_v corresponding to E_3 reaches its maximum, nearly 6.36 times the initial value, while that corresponding to E_2 and E_4 achieves a stable state, with an equilibrium value but less than E_3. It reflects that when the swell partition and the wind-sea partition are separated (i.e., ID > 0.10), the third-order nonlinearity weakens, with minimal impact on the second-order and the fourth-order nonlinearity, indicating that the increased energy of the third-order nonlinearity mainly comes from the interaction between wave groups. Meanwhile, compared to the linear components, the fourth-order components are pointed out to be reduced by three orders of magnitude, while the second-order components are reduced by only one order of magnitude,[47,48] which can also be observed in our nonlinear analysis of wavenumber-frequency spectra given in Fig. 13 (Appendix C). Suppose that the fourth-order components are too little to be taken note of the energy of the second-order difference is stronger than that of the second-order sum.

Concerning the variation with SEER [Fig. 9(b)], the overall trend is that increases rapidly and then decreases slowly, and the increased magnitude of the third-order components relative to that of the second-order difference components is also more significant. Near the point at SSER = 0.67, which seems a swell-dominated state, the maximum values of the energy from the high-order components emerge. Till SSER = 1.50, a steady state is obtained for the energy amplification of nonlinear harmonics. This phenomenon may be a little different from our previous study,[30] in which the wave configuration with wind-sea-swell equivalent has the weakest nonlinearity, explained by the fact that the value of the intermodal distance is not the same.

3. Energy difference before and after focusing

As defined in Eq. (10), E_d measures the difference between the harmonical energy at the position behind and before the focused position. The corresponding variations in different sea states are presented in Fig. 10. A quite attractive phenomenon is that the energy difference of E_1 and E_3 is always negative and that of E_2 and E_4 are positive. This means that after the evolution of double-wave-group focusing, the energy of odd-order components is being transferred to even-order components.

Although the third-order energy is intensively active as the swell waves collide with the wind-sea waves [Fig. 9(a)], there are quite tiny energy differences of E_3 [Fig. 10(a)], suggesting that the third-order nonlinear interaction is mainly triggered by the transient effect of the wave focusing rather than a long-term evolution. For various values of ID, the energy difference of even-order components (i.e., the red line and the orange line) always remains at a higher level, that is, the energy
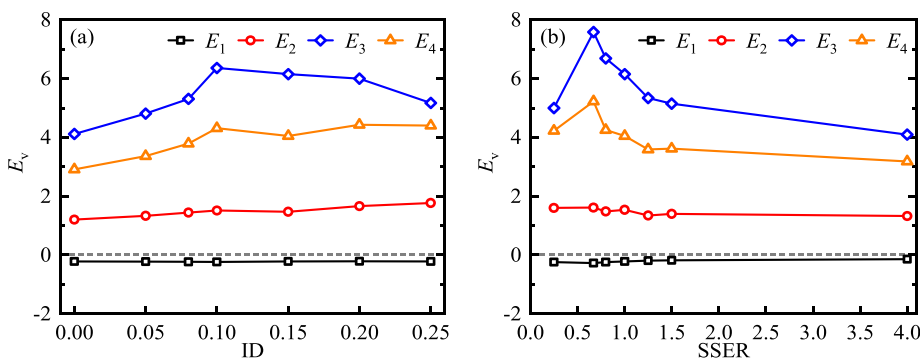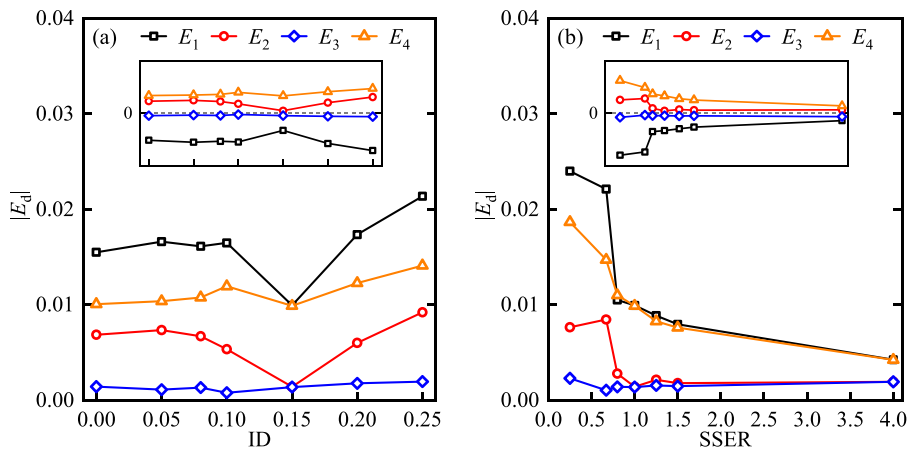
FIG. 10. Proportion of the harmonical energy difference before and after the wave group focusing in various sea states, (a) with various values of ID and (b) with various values of SSER.

of even-order components is almost going with the entire evolution process. Moreover, as the intermodal distance enlarges, the interactions between the swell and wind-sea decay, and the nonlinear energy difference take on a decreasing trend. When ID > 0.15, owing to the enhancement of the wave steepness in wind-sea waves, the energy difference rises again.

In Fig. 10(b), the energy differences between E_2 and E_4 dramatically reduce as the energy of the wind-sea system increases (i.e., the value of SSER increases), still over that of E_3. This implies again that the even-order interaction, especially the second-order difference impact, dominates the energy difference before and behind the focusing. The maximum amplification during the harmonic evolution and the energy difference before and after focusing reach their maximum value in the swell-dominated state (SSER < 1.00), respectively. Then, the nonlinear interaction and energy transfer are impaired with the energy of the wind-sea increasing (SSER ≥ 1.00). Interestingly, in the sea states with swell and wind-sea equivalent (i.e., SSER = 1.00) and dominated by wind-sea (i.e., SSER > 1.00), the energy difference of E_1 is equal to that of E_4, and so is the difference of E_3 and E_2. That is to say, at this moment, the linear components tend to transfer to the second-order difference, and the third-order to the second-order sum, revealing a pattern of energy transfer that energy inclines to move to a lower frequency band.

The phenomenon with unequal energy distribution at the symmetric position before and behind the focused position confirms that some new frequency components are generated in the process of the wave focusing and wave defocusing, resulting in the variation of the dispersion relation given in Fig. 13 (Appendix C).

V. CONCLUSIONS

In this paper, the spatial evolution of the double-wave-group focusing is numerically simulated based on a fully nonlinear wave tank. Variations of time and frequency characteristics and the energy transfer properties are analyzed. The main conclusions are as follows:

(1) The closer the intermodal distance (ID), the more disequilibrium the spectral distribution, and the larger the focused amplitude. The focused amplitude of double-wave-group focusing relative to that of the linear superposition of the corresponding single-wave-group focusing, namely, $(\eta_{AB})/(\eta_{A+B})$, decreases monotonously with the increase of ID but first reduces and

then increases with the increase of the sea-swell energy ratio, with the minimum in the sea-swell energy equivalent state (i.e., SSER = 1.00).

(2) The evolution of the nonlinear energies is not a symmetrical process. They begin to be activated at a position three times the characteristic wavelength before the focus. Then, they achieve their maximum value near the focus, but not yet exactly at it. After that, they tend to revert to their symmetrical state but actually do not. Additionally, the third-order nonlinear interaction is primarily triggered by the transient effect of the wave focusing, rather than a long-term evolution like that of the even-order components.

(3) In a state with a closer intermodal distance (i.e., ID < 0.10) or one that is swell-dominated (i.e., SSER < 1.00), the strongest nonlinear energy occurs behind the actual focused position. Conversely, in other states, it occurs forward. The greatest deviation relative to the actual focused position occurs in the swell-sea energy equivalent state (i.e., SSER = 1.00).

(4) A configuration with an ID of 0.10 or a swell-dominated state with an SSER of 0.67 is more likely to amplify the nonlinear energy, with a magnification factor of 6.36 or 7.58 for E_3, respectively. For other configurations with an ID greater than 0.15, the energy amplification of even-order harmonics tends to stabilize, while that of third-order harmonics gradually decreases.

(5) The energy asymmetry before and after the wave focus indicates an irreversible energy transfer from a relatively higher frequency to a nearby lower frequency. The sea state with a wider intermodal distance (i.e., ID > 0.10) or swell-dominated (i.e., SSER < 1.00) increases the initial energy in the system with a relatively lower frequency. This suggests that the bound waves activated by the amplitude modulation promote a pattern where linear components transfer to the second-order difference and the third-order to the second-order sum.

These findings enhance our understanding of the configuration under which large waves are more likely to occur, thereby contributing to the knowledge of extreme wave generation. The ability to quickly identify configurations that are more likely to trigger larger waves can guide practical engineering decisions, such as the placement of marine structures and the planning of shipping routes.

In conclusion, the energy transfer in the spatial evolution of a double-wave-group focusing in a uni-directional sea configuration is clarified. In real sea states, waves are distributed not only in the frequency domain but also in the spreading direction. Future research based on this work will investigate two wave groups with different propagation directions in a three-dimensional wave basin. This will likely uncover a multitude of unknown but fascinating physical phenomena.

AUTHOR DECLARATIONS
Conflict of Interest

The authors have no conflicts to disclose.

Author Contributions

Binzhen Zhou: Conceptualization (equal); Funding acquisition (equal); Project administration (equal); Supervision (equal); Writing—review & editing (equal). **Kanglixi Ding:** Conceptualization (equal); Data curation (lead); Investigation (lead); Methodology (equal); Visualization (equal); Writing—original draft (lead). **Yi Xiao:** Formal analysis (equal); Investigation (equal); Writing—review & editing (equal). **Lei Wang:** Conceptualization (lead); Formal analysis (equal); Funding acquisition (equal); Methodology (lead); Writing—review & editing (lead). **Tianning Tang:** Investigation (equal); Writing—review & editing (equal).

DATA AVAILABILITY

The data that support the findings of this study are available from the corresponding author upon reasonable request.

APPENDIX A: VALIDATION OF THE ITERATIVE METHOD TO GENERATE WAVES

To assess the quality of the corrected waves based on the iterative method, a peak performance (PPS) is introduced, expressed as[49]

$$\text{PPS} = \left(1 - \frac{(\eta_{\text{linear}_{\max}} - \eta_{\text{target}_{\max}})^2}{\eta_{\text{target}_{\max}}^2}\right) \times 100\%, \quad \text{(A1)}$$

where $\eta_{\text{target}_{\max}}$ is the assumed focused amplitude (i.e., target focused amplitude), and $\eta_{\text{linear}_{\max}}$ represents the measured water surface elevation corresponding to the focused position of the linear components, which are obtained through the four-phase decomposition method.[21]
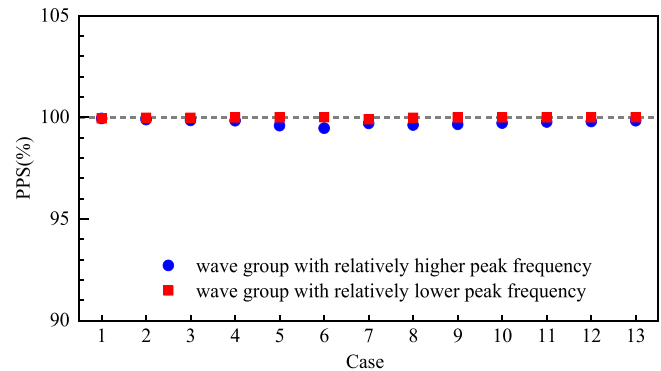

FIG. 11. Peak performance of the iterative methods applied in various wave conditions in our study.

PPS of each configuration listed in Table I is given in Fig. 11, where the blue circles and the red triangles denote the cases with relatively higher peak frequency and those with relatively low peak frequency, respectively. The results show that the overall PPS can achieve a value of more than 99.5%, implying that the shift of focused position can be accurately eliminated by this empirical methodology.

APPENDIX B: VALIDATION OF THE NUMERICAL MODAL BASED ON HOS-NWT

To verify the accuracy of the established numerical model, physical experiments are conducted in the wave flume at the Ship and Ocean Engineering Laboratory, South China University of Technology, China. The wave flume is 32 m long, 1 m wide, and 1.5 m deep. The working water depth is kept at 1.0 m. 3 wave gauges are located before, at, and behind the focused position. The configuration can be referred to case 4 (ID = 0.10, SSER = 1.00) as listed in Table I. Concerning our numerical simulation using HOS-NWT, the comparison of wave surface elevation between numerical results and experimental data given in Fig. 12 shows a quite good agreement, demonstrating that the numerical model can accurately simulate the evolution of double-wave-group focusing.

APPENDIX C: EVOLUTION OF WAVENUMBER-FREQUENCY SPECTRA

The wavenumber–frequency (k–f) spectrum specializes in the analysis of the time-frequency characteristics, including the evolution of the amplitude spectra and changes in the dispersive properties of the wave groups.[50] It can be obtained by 2D short-time Fourier transform,[22] written as

$$\text{ST}(\tau, f) = \int_{-\infty}^{\infty} x(t) \frac{f}{\sqrt{2\pi}} e^{-((\tau-t)^2 f^2/2)} e^{(-\text{i}2\pi ft)} \mathrm{d}t. \quad \text{(C1)}$$

Additionally, for a free wave group, the frequency f_i and the wavenumber k_i satisfy

$$(2\pi f_i)^2 = gk_i \tanh(k_i h), \quad \text{(C2)}$$
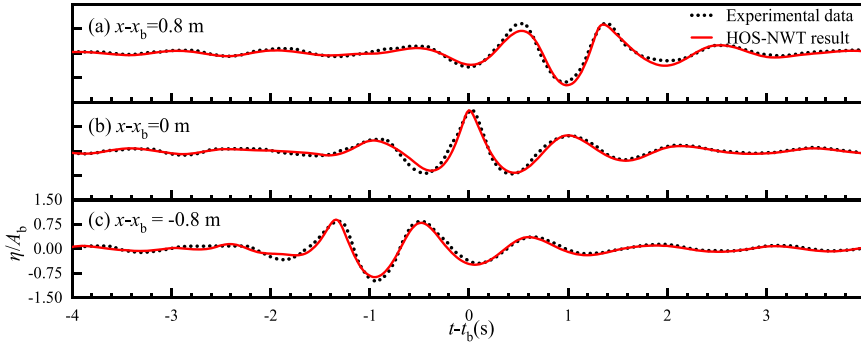
where h is the water depth.

FIG. 12. Comparison of free surface elevations between numerical results and experimental along the wave propagation (case 4 ID = 0.1, SSER = 1.0).

For the nth order free sup-harmonics, the dispersive relation can be written as[51]

$$(2n\pi f_i)^2_{\mathrm{H}} = ngk_i \tanh(nk_i h).$$ (C3)

For the nth order bound sub-harmonics, their wavenumbers obey the relation expressed as[51]

$$(2n\pi f_i)^2_{\mathrm{L}} = gk_i \tanh(k_i h).$$ (C4)

Figure 13 illustrates the evolution of the wavenumber-frequency spectrum corresponding to each harmonic, in which $a_{\max}$ is the maximum amplitude in the frequency domain. The red, blue, and green dash lines denote the dispersion relation of the second-order bound sub-harmonics [obtained from Eq. (C4)], linear

components [obtained from Eq. (C2)], and second-order free super-harmonics [obtained from Eq. (C3)], respectively, with the corresponding frequency spectra given on the left. During the propagation of the wave groups, the variations in the energy of different harmonics are quite different. Only at the focused position (i.e., there is a most intense interaction between swell waves and the wind-sea waves), fewer fourth-order components appeared in the upper right corner in Fig. 13(b.4), indicating that throughout the evolutionary process, the energy of the fourth-order harmonics is so low that it can be ignored. That is to say, E_4 can be considered as being composed of energy mainly from the second-order difference harmonics. Additionally, compared with the initial state of the wave evolution in Fig. 13(a), the deviation from the theoretical nonlinear dispersion relation enlarges in Fig. 13(c), resulting in
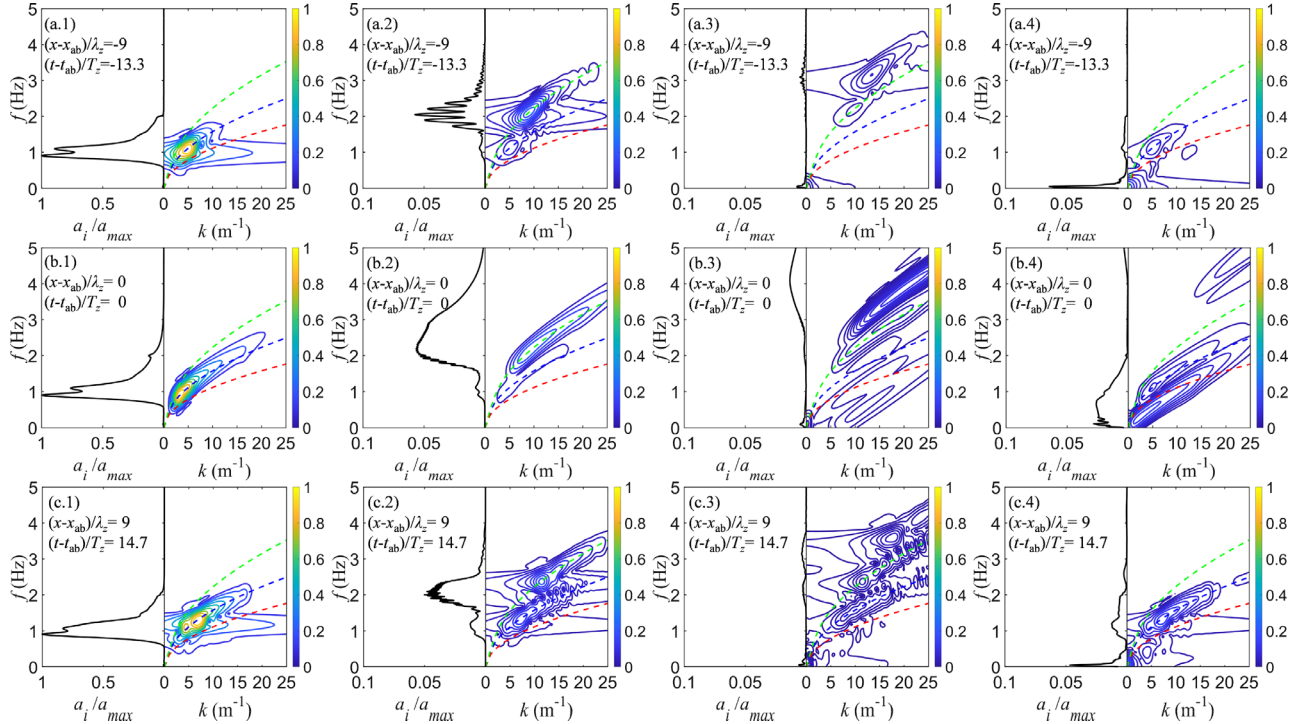

FIG. 13. Wavenumber-frequency spectra of harmonical signals (case 4 ID = 0.10, SSER = 1.00). (a) Before the focused position, (b) at the focused position, and (c) behind the focused position. (1) Linear energy (E_1), (2) second-order sum energy (E_2), (3) third-order energy (E_3), and (4) second-order difference and fourth-order energy (E_4).

differences such as the enhancement of the high-frequency tail of the linear components and the expansion of the distribution range of the even-order components.

REFERENCES

[1]B. Zhou, K. Ding, J. Wang et al., "Experimental study on the interactions between wave groups in double-wave-group focusing," Phys. Fluids **35**(3), 037118 (2023).

[2]R. Vettor and C. Soares, "A global view on bimodal wave spectra and crossing seas from ERA-interim," Ocean Eng. **210**, 107439 (2020).

[3]K. Dysthe, H. Krogstad, and P. Müller, "Oceanic rogue waves," Annu. Rev. Fluid Mech. **40**, 287–310 (2008).

[4]E. Didenkulova, I. Didenkulova, and I. Medvedev, "Freak wave events in 2005–2021: Statistics and analysis of favourable wave and wind conditions," Nat. Hazards Earth Syst. Sci. **23**(4), 1653–1663 (2023).

[5]D. Häfner, J. Gemmrich, and M. Jochum, "Real-world rogue wave probabilities," Sci. Rep. **11**(1), 10084 (2021).

[6]M. Onorato, A. Osborne, and M. Serio, "Modulational instability in crossing sea states: A possible mechanism for the formation of freak waves," Phys. Rev. Lett. **96**(1), 014503 (2006).

[7]C. Kharif and E. Pelinovsky, "Physical mechanisms of the rogue wave phenomenon," Eur. J. Mech., B **22**(6), 603–634 (2003).

[8]S. Draycott, Y. Li, P. Stansby et al., "Harmonic-induced wave breaking due to abrupt depth transitions: An experimental and numerical study," Coastal Eng. **171**, 104041 (2022).

[9]K. Trulsen, H. Zeng, and O. Gramstad, "Laboratory evidence of freak waves provoked by non-uniform bathymetry," Phys. Fluids **24**(9), 097101 (2012).

[10]Y. Ma, G. Dong, M. Perlin et al., "Laboratory observations of wave evolution, modulation and blocking due to spatially varying opposing currents," J. Fluid Mech. **661**, 108–129 (2010).

[11]L. Chen, D. Stagonas, H. Santo et al., "Numerical modelling of interactions of waves and sheared currents with a surface piercing vertical cylinder," Coastal Eng. **145**, 65–83 (2019).

[12]T. Benjamin and J. Feir, "The disintegration of wave trains on deep water Part 1. Theory," J. Fluid Mech. **27**(3), 417–430 (1967).

[13]A. Sarkar and A. Chanda, "Structural performance of a submerged bottom-mounted compound porous cylinder on the water wave interaction in the presence of a porous sea-bed," Phys. Fluids **34**(9), 092113 (2022).

[14]K. Barman, A. Chanda, C. Tsai et al., "Bragg scattering of gravity waves by a sea bed of varying depth in the presence of uniform current covered by a floating membrane," Phys. Fluids **36**(1), 012118 (2024).

[15]X. Li, X. Li, and S. Liao, "Pattern transition of two-dimensional Faraday waves at an extremely shallow depth," Sci. China Phys. Mech. Astron. **59**, 1–3 (2016).

[16]X. Li, X. Li, S. Liao, et al., "Effect of width on the properties of Faraday waves in Hele–Shaw cells," Sci. China Phys. Mech. Astron. **62**(7), 974711 (2019).

[17]R. Rapp and W. Melville, "Laboratory measurements of deep-water breaking waves," Philos. Trans. R. Soc. London, Ser. A **331**(1622), 735–800 (1990).

[18]T. Baldock, C. Swan, and P. Taylor, "A laboratory study of nonlinear surface waves on water," Philos. Trans. R. Soc. London, Ser. A **354**(1707), 649–676 (1996).

[19]T. Adcock and P. Taylor, "Non-linear evolution of uni-directional focused wave-groups on a deep water: A comparison of models," Appl. Ocean Res. **59**, 147–152 (2016).

[20]E. Buldakov, D. Stagonas, and R. Simons, "Extreme wave groups in a wave flume: Controlled generation and breaking onset," Coastal Eng. **128**, 75–83 (2017).

[21]C. Fitzgerald, P. Taylor, R. Taylor et al., "Phase manipulation and the harmonic components of ringing forces on a surface-piercing column," Proc. R. Soc. A **470**(2168), 20130847 (2014).

[22]C. Bayındır, "Early detection of rogue waves by the wavelet transforms," Phys. Lett. A **380**(1–2), 156–161 (2016).

[23]R. Gibson and C. Swan, "The evolution of large ocean waves: The role of local and rapid spectral changes.," Proc. R. Soc. A **463**(2077), 21–48 (2007).

[24]O. Gramstad and K. Trulsen, "Fourth-order coupled nonlinear Schrödinger equations for gravity waves on deep water," Phys. Fluids **23**(6), 062102 (2011).

[25]J. Li, J. Yang, S. Liu et al., "Wave groupiness analysis of the process of 2D freak wave generation in random wave trains," Ocean Eng. **104**, 480–488 (2015).

[26]C. Cui and W. Pan, "Experimental study on the wavelengths of two-dimensional and three-dimensional freak waves," China Ocean Eng. **37**(1), 154–164 (2023).

[27]A. Tao, J. Zheng, B. Chen et al., "Properties of freak waves induced by two kinds of nonlinear mechanisms," Int. Conf. Coastal Eng. **1**(33), 73 (2012).

[28]S. Liu, T. Waseda, J. Yao et al., "Statistical properties of surface gravity waves and freak wave occurrence in crossing sea states," Phys. Rev. Fluids **7**(7), 074805 (2022).

[29]M. McAllister, S. Draycott, T. Adcock et al., "Laboratory recreation of the Draupner wave and the role of breaking in crossing seas," J. Fluid Mech. **860**, 767–786 (2019).

[30]L. Wang, J. Li, S. Liu et al., "Statistics of long-crested extreme waves in single and mixed sea states," Ocean Dyn. **71**, 21–42 (2021).

[31]G. Rodriguez, C. Soares, M. Pacheco et al., "Wave height distribution in mixed sea states," J. Offshore Mech. Arct. Eng. **124**(1), 34–40 (2002).

[32]F. Arena and C. Soares, "Nonlinear high wave groups in bimodal sea states," J. Waterw., Port, Coastal, Ocean Eng. **135**(3), 69–79 (2009).

[33]O. Gramstad and K. Trulsen, "Can swell increase the number of freak waves in a wind sea?," J. Fluid Mech. **650**, 57–79 (2010).

[34]L. Wang, K. Ding, B. Zhou et al., "Quantitative prediction of the freak wave occurrence probability in co-propagating mixed waves," Ocean Eng. **271**, 113810 (2023).

[35]L. Wang, K. Ding, B. Zhou et al., "Nonlinear statistical characteristics of the multi-directional waves with equivalent energy," Phys. Fluids **35**(8), 087101 (2023).

[36]L. Wang, J. Li, S. Liu et al., "Experimental and numerical studies on the focused waves generated by double wave groups," Front. Energy Res. **8**, 133 (2020).

[37]L. Wang, B. Zhou, P. Jin et al., "Relation between occurrence probability of freak waves and kurtosis/skewness in unidirectional wave trains under single-peak spectra," Ocean Eng. **248**, 110813 (2022).

[38]G. Ducrozet, M. Abdolahpour, F. Nelli et al., "Predicting the occurrence of rogue waves in the presence of opposing currents with a high-order spectral method," Phys. Rev. Fluids **6**(6), 064803 (2021).

[39]G. Ducrozet, F. Bonnefoy, D. Le Touzé et al., "A modified high-order spectral method for wavemaker modeling in a numerical wave tank," Eur. J. Mech., B **34**, 19–34 (2012).

[40]F. Bonnefoy, G. Ducrozet, D. Le Touzé et al., "Time domain simulation of nonlinear water waves using spectral methods," in Advances in Numerical Simulation of Nonlinear Water Waves (World Scientific Publishing, 2010), pp. 129–164.

[41]G. Dommermuth and P. Yue, "A high-order spectral method for the study of nonlinear gravity waves," J. Fluid Mech. **184**, 267–288 (1987).

[42]B. J. West, K. A. Brueckner, R. S. Janda et al., "A new numerical method for surface hydrodynamics," J. Geophys. Res. **92**(C11), 11803–11824, https://doi.org/10.1029/JC092iC11p11803 (1987).

[43]Y. Agnon and B. Bingham, "A non-periodic spectral method with application to nonlinear water waves," Eur. J. Mech., B **18**(3), 527–534 (1999).

[44]R. Sobey, "The distribution of zero-crossing wave heights and periods in a stationary sea state," Ocean Eng. **19**(2), 101–118 (1992).

[45]D. Ning, C. Liang, L. Chen et al., "Numerical investigation on the propagation and evolution of focused waves over a sloping bed," Ocean Eng. **250**, 111035 (2022).

[46]B. Zhou, K. Ding, J. Huang et al., "Influence of uniform currents on nonlinear characteristics of double-wave-group focusing," Phys. Fluids **36**(3), 037125 (2024).

[47]X. Feng, P. Taylor, S. Dai et al., "Experimental investigation of higher harmonic wave loads and moments on a vertical cylinder by a phase-manipulation method," Coastal Eng. **160**, 103747 (2020).

[48]L. Chen, J. Zang, P. Taylor et al., "An experimental decomposition of nonlinear forces on a surface-piercing column: Stokes-type expansions of the force harmonics," J. Fluid Mech. **848**, 42–77 (2018).

[49]Y. Ma, B. Tai, G. Dong et al., "An experiment on reconstruction and analyses of in-situ measured freak waves," Ocean Eng. **244**, 110312 (2022).

[50]I. Redor, E. Barthélemy, H. Michallet et al., "Experimental evidence of a hydrodynamic soliton gas," Phys. Rev. Lett. **122**(21), 214502 (2019).

[51]J. Zhang, M. Benoit, and Y. Ma, "Equilibration process of out-of-equilibrium sea-states induced by strong depth variation: Evolution of coastal wave spectrum and representative parameters," Coastal Eng. **174**, 104099 (2022).